



Flexible modification and texture prediction and control method of internal gearing power honing tooth surface

Jian-Ping Tang¹ · Jiang Han¹ · Xiao-Qing Tian¹ · Zhen-Fu Li¹ · Tong-Fei You¹ · Guang-Hui Li¹ · Lian Xia¹

Received: 27 June 2023 / Revised: 17 August 2023 / Accepted: 25 March 2024

© Shanghai University and Periodicals Agency of Shanghai University and Springer-Verlag GmbH Germany, part of Springer Nature 2024

Abstract High precision and minimal noise are considered critical performance measures for top-tier gear transmission systems. To ensure optimum gear transmission performance, the tooth surface texture should be enhanced without comparing the gear precision. By integrating the principle of internal gearing power honing with tooth surface topology modifications, the adjusted honing texture can be forecasted, and proactive control can be achieved, both of which are considered as crucial for the reduction of gear vibration and noise. In this study, a manufacturing technique for high-order modified helical gears is introduced. The formation rules and modeling of the honing texture are explored, leading to a novel method for three-dimensional modeling and control of the altered honing texture. The direction of the cutting speed of abrasive grains at the contact point between the honing wheel and working gear tooth surface was examined. Using the discrete abrasive grain motion trajectory method, the honing texture was produced, through which the formation mechanisms and control strategies of the curved honing texture were illuminated. Based on these findings, a method for flexible topology modifications of the tooth surface is suggested. This is achieved by adjusting the motion coefficients of each axis of the honing machine and adding additional motion in the form of higher-order polynomials to three motion axes, including the radial feed and oscillation axes of the honing wheel and the interleaved axes of the work gear and honing wheel. A least-squares estimation method,

based on a sensitivity matrix, was employed to determine the additional motion coefficients. By this method, the texture of the modified tooth surface can also be predicted and controlled. In a numerical example, the efficacy of the flexible topology modification method was confirmed. In this case, the altered honing texture was managed by modifying the axis intersection angle, while the accuracy of tooth surface modifications was maintained. This study has theoretical and application value in the field of gear manufacturing, oriented to the demand for gear vibration and noise reduction functions.

Keywords Internal gearing power honing · Honing texture · Texture modulation · Topology modification · Sensitivity matrix

1 Introduction

Gears are pivotal transmission components in high-end machinery and equipment, playing a crucial role in determining the performance and reliability of these machines [1]. Currently, the trend in gear manufacturing leans toward high precision, low noise, increased strength, and lightweight design, especially in the realm of new energy vehicles which demand stricter noise reduction from gears [2]. The primary sources of gear noise can be traced back to two key aspects: the gear's macrogeometry and microgeometry. Although macrogeometry pertains to the overall shape of the gear, microgeometry focuses on its surface morphology. Previous studies indicated that modifications to the gear's macrogeometry and controls over its microgeometry could lead to enhanced tooth contact and transmission performance, consequently diminishing gear vibration and transmission noise [3–5].

✉ Jiang Han
Jianghan@hfut.edu.cn

✉ Xiao-Qing Tian
tianxiaqing@hfut.edu.cn

¹ School of Mechanical Engineering, Hefei University of Technology, Hefei 230009, People's Republic of China

Internal gearing power honing serves as the final step in the processing of high-precision, low-noise gears. This technique not only reduces the manufacturing costs of high-precision gears but also enhances both the tooth surface accuracy and texture [6]. Unlike grinding textures, honing textures are characterized by an arc distribution on both sides of the pitch circle. This irregular tooth surface texture aids in preventing periodic resonance, leading to a notable reduction in noise during gear operation [7–9]. Thus, it becomes imperative to investigate the formation mechanism of the honing texture using 3D modeling to facilitate the design and optimization of noise reduction in gears. Many researchers have established a correlation between the morphology of the grinding wheel and that of the workpiece for 3D modeling of surface grinding texture. For instance, Chen et al. [10] employed a moving average model to recreate the observed worm wheel surface morphology. This reconstructed morphology was then mapped onto the 3D surface of the workpiece using the abrasive grain trajectory equation. Miller et al. [11, 12] introduced a simulation model for the morphology of surface grinding based on a Fourier forward and inverse transform derived from a wheel morphology model. However, due to differences in machining principles and workpiece geometry, the prediction model for gear surface morphology diverges from the flat-grinding morphology prediction model. Zhou et al. [13] formulated a 3D model to anticipate the grinding trajectory and interference regions arising from gear grinding. This was achieved by reconstructing the worm wheel morphology to forecast the tooth surface morphology along the tooth profile direction. Yang et al. [14] constructed a grinding texture by determining the trajectory of the grinding grains and resolving the interference region. The honing texture angle was controlled by adjusting an additional installation angle between the grinding wheel and work gear shaft. Nevertheless, the honing tooth surfaces exhibit an irregular, asymmetrical curved texture. This complexity implies that equations delineating the trajectory of the grinding grains are intricate to decipher, rendering the modeling of the honing texture and its control methodologies challenging to execute.

As highlighted earlier, regulating the honing texture on a microscopic scale is crucial for reducing gear vibration and noise. Moreover, gear shapes can be adapted on a macroscopic scale using topology modification. This adjustment aids in avoiding stress concentration at the meshing gear pair's top and root and minimizing edge contact, leading to decreased load fluctuation, vibration, and noise during gear transmission [15–17]. In recent times, flexible topology modifications have garnered considerable attention. Unlike the traditional approach, which mandates altering the dressing tool's contour to achieve desired topology effects, flexible topology

modification is a motion-controlled method. This method alters the tool trajectory during machining to obtain various topology effects without the need for a new dressing tool, offering superior modification accuracy [18]. Shih and Chen [19] and Shin and Fong [20] proposed a method to modify the tooth surfaces of gears using a five-axis CNC grinder. In this method, each machine axis is manipulated by a higher-order polynomial to tailor the gear pair's tooth surfaces, aiming to attain the optimal shape derived from experiential approximations. However, both domestically and internationally, the focus on the topology modification of tooth profiles during gear honing has been limited. Han et al. [21] introduced an electronic gearbox control-based approach for honing tooth topology modification. This method defines the motion of two rotating axes as a fourth-order polynomial function relative to the axial feed of the honing wheel, achieving topology modification through inter-axis linkage. Yu et al. [22] presented a worm-honing inter wheel tooth-honing modification technique, employing motion control to realize arbitrary gear alterations. Based on numerical simulations, Tran and Wu [23] confirmed that the tooth surface method of topology modification, grounded in multi-axis linkage control, outperformed traditional methods in flexibility and utility. However, the effects of higher-order topology modifications can differ based on machine axis configurations, influencing the honing tooth surface in varied ways. Furthermore, research on modified honing texture has not been explored, to date.

Although honing machines are commonly employed in the machining process of precision gears, much of the research on honing has predominantly centered on theoretical studies concerning gear finishing. For the first time, this study introduces a method to predict the three-dimensional texture of tooth surfaces. This method facilitates texture prediction and control of modified tooth surfaces, leveraging existing high-precision flexible modification techniques. The research also offers guidance on determining gear macro and microstructures and analyzing the gear contact signal induced by honed gear surfaces, by passing the need for practical experimental tests. In this approach, the honing texture is predicted by determining the cutting velocity direction at the contact point between the honing wheel and the work gear through the discrete abrasive grain motion trajectory method. Furthermore, the influence of the variable axis intersection angle on the honing texture direction is examined to ensure that tooth surface accuracy remains unaffected. A method is presented that adjusts the motion coefficients of each machine axis on the honing machine, aiming to achieve flexible topology modification of the tooth surface. The 3D model of the modified honing texture and its control method are predicted, ensuring consistent tooth surface accuracy. In conclusion, the efficiency of the modification method, the predictive model for the modified

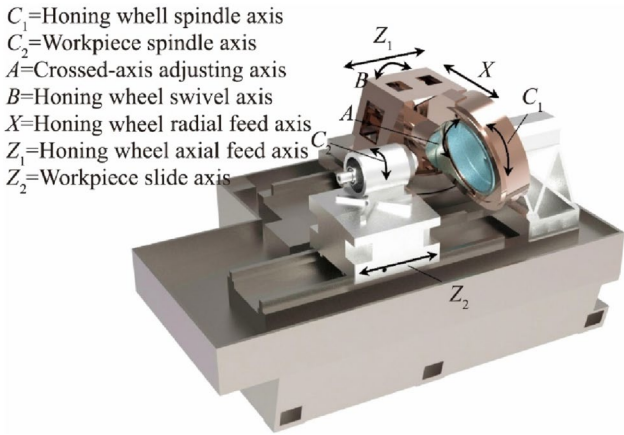


Fig. 1 Y4830 CNC internal gearing power honing machine

honing texture, and the control method are verified using numerical examples.

2 Mathematical modeling for internal gearing power honing

Figure 1 illustrates the construction and machining axes of the internal gearing power honing machine. The machine features seven CNC axes: four rotary axes (C_1 , C_2 , A , and B) and three translational axes (X , Z_1 , and Z_2). The honing procedure comprises two main stages: dressing the honing wheel and executing the gear honing. Initially, a diamond dressing wheel, mirroring the profile of the work gear, is utilized to shape the honing wheel's profile through a continuous spreading dressing process. Following this, the honing wheel performs the spreading honing to produce the work-gear profile. This section delves into the motion interplay among these machining axes during the honing wheel dressing and gear honing stages.

2.1 Dressing of honing wheels

Figure 2 illustrates the corresponding coordinate systems for the dressing process of the honing wheel. The coordinate systems $S_d(x_d, y_d, z_d)$ and $S_h(x_h, y_h, z_h)$ are fixed to the diamond dressing wheel and honing wheel, respectively. Furthermore, $S_1(x_1, y_1, z_1)$ and $S_2(x_2, y_2, z_2)$ denote auxiliary coordinate systems for homogenous coordinate transformation. According to the principle of involute helical surface formation, the position vector r_d and normal vector n_d of any point M on the tooth surface of the diamond dressing wheel in the coordinate system can be expressed as Eqs. (1) and (2) [24].

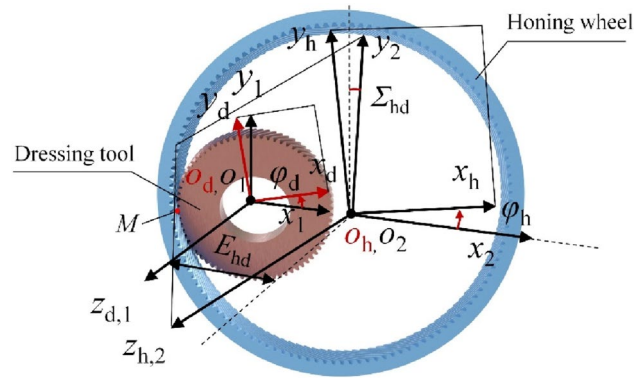


Fig. 2 Coordinate system of relative motion between diamond dressing wheel and honing wheel

$$r_d = \begin{bmatrix} r_b \cos(\sigma_0 + \theta + \lambda) + r_b \lambda \sin(\sigma_0 + \theta + \lambda) \\ r_b \sin(\sigma_0 + \theta + \lambda) - r_b \lambda \cos(\sigma_0 + \theta + \lambda) \\ p\theta \\ 1 \end{bmatrix}, \quad (1)$$

where r_b denotes the base radius of the dressing wheel; p denotes the helix parameter, $p = r_{d1}/\tan\beta_d$; r_{d1} denotes the operating pitch radius; β_d denotes the pitch helix angle; θ denotes the helix increment angle; σ_0 denotes the involute starting angle; and λ denotes the involute increment angle. The position vector r_h and normal vector n_h of the surface of the honing wheel were determined by the homogenous coordinate transformation from S_d to S_h

$$n_d = \lambda r_b \begin{bmatrix} p \sin(\sigma_0 + \theta + \lambda) \\ -p \cos(\sigma_0 + \theta + \lambda) \\ r_b \end{bmatrix}, \quad (2)$$

$$r_h(\varphi_d, \theta, \lambda) = M_{hd}(\varphi_d) \cdot r_d(\theta, \lambda), \quad (3)$$

$$n_h(\varphi_d, \theta, \lambda) = L_{hd}(\varphi_d) \cdot n_d(\theta, \lambda), \quad (4)$$

$$M_{hd}(\varphi_d) = M_{h2}(\varphi_h) \cdot M_{21} \cdot M_{1d}(\varphi_d), \quad (5)$$

where

$$M_{1d} = \begin{bmatrix} \cos \varphi_d & -\sin \varphi_d & 0 & 0 \\ \sin \varphi_d & \cos \varphi_d & 0 & 0 \\ 0 & 0 & 1 & 0 \\ 0 & 0 & 0 & 1 \end{bmatrix},$$

$$M_{21} = \begin{bmatrix} 1 & 0 & 0 & -E_{hd} \\ 0 & \cos \Sigma_{hd} & \sin \Sigma_{hd} & 0 \\ 0 & -\sin \Sigma_{hd} & \cos \Sigma_{hd} & 0 \\ 0 & 0 & 0 & 1 \end{bmatrix}, M_{h2} = \begin{bmatrix} \cos \varphi_h & \sin \varphi_h & 0 & 0 \\ -\sin \varphi_h & \cos \varphi_h & 0 & 0 \\ 0 & 0 & 1 & 0 \\ 0 & 0 & 0 & 1 \end{bmatrix};$$

M_{hd} denotes the coordinate transformation matrix from coordinate system S_d to S_h ; L_{hd} is transformed to M_{hd} to remove the submatrix of the last row and column; φ_d and φ_h denote the rotation angles of the dressing wheel and honing

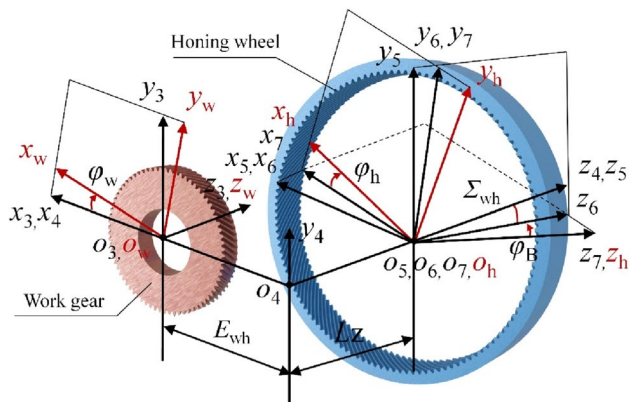


Fig. 3 Coordinate system of relative motion of honing wheel and work gear

wheel, respectively; and E_{hd} denotes the center distance between the whole wheel and honing wheel. Furthermore, Σ_{hd} denotes the axis intersection angle of the diamond dressing wheel and honing wheel, and the calculation method is

$$\varphi_h = \varphi_d N_d / N_h, \tag{6}$$

$$E_{hd} = r_{h1} - r_{d1}, \tag{7}$$

$$\Sigma_{hd} = \beta_h \pm \beta_d, \tag{8}$$

where N_d and N_h denote the number of teeth of the dressing and honing wheels, respectively; r_{h1} denotes the operating pitch radii of the honing wheel and β_h denotes the helix angles of the honing wheel. Furthermore, “ \pm ” symbol indicates whether the helix angle of the honing wheel and dressing wheel is in the same direction ($-$) or in the opposite direction ($+$). According to the gear meshing principle, the meshing equations for the honing wheel and diamond-dressing gear can be obtained [21]

$$f_1(\varphi_d, \theta, \lambda) = \mathbf{n}_h(\varphi_d, \theta, \lambda) \cdot \frac{\partial \mathbf{r}_h(\varphi_d, \theta, \lambda)}{\partial \varphi_d} = 0. \tag{9}$$

2.2 Generating honing of gear

The corresponding coordinate systems for the honing process of gear are shown in Fig. 3. $S_h(x_h, y_h, z_h)$ and $S_w(x_w, y_w, z_w)$ are fixed to the honing wheel and work gear, respectively. Furthermore, $S_3(x_3, y_3, z_3)$, $S_4(x_4, y_4, z_4)$, $S_5(x_5, y_5, z_5)$, $S_6(x_6, y_6, z_6)$, and $S_7(x_7, y_7, z_7)$ are auxiliary coordinate systems for the homogenous coordinate transformation. The position vector \mathbf{r}_w and normal vector \mathbf{n}_w of the tooth face are represented in the coordinate system.

$$\mathbf{r}_w(L_z, \varphi_h, \varphi_d, \theta, \lambda) = \mathbf{M}_{wh}(L_z, \varphi_h) \cdot \mathbf{r}_h(\varphi_d, \theta, \lambda), \tag{10}$$

$$\mathbf{n}_w(L_z, \varphi_h, \varphi_d, \theta, \lambda) = \mathbf{L}_{wh}(L_z, \varphi_h) \cdot \mathbf{n}_h(\varphi_d, \theta, \lambda), \tag{11}$$

$$\mathbf{M}_{wh}(L_z, \varphi_h) = \mathbf{M}_{w3} \cdot \mathbf{M}_{34} \cdot \mathbf{M}_{45} \cdot \mathbf{M}_{56} \cdot \mathbf{M}_{67} \cdot \mathbf{M}_{7h}, \tag{12}$$

$$\begin{matrix} w & & h & & e & & r & & e \\ \mathbf{M}_{7h} = \begin{bmatrix} \cos \varphi_h & -\sin \varphi_h & 0 & 0 \\ \sin \varphi_h & \cos \varphi_h & 0 & 0 \\ 0 & 0 & 1 & 0 \\ 0 & 0 & 0 & 1 \end{bmatrix}, & \mathbf{M}_{67} = \begin{bmatrix} \cos \varphi_B & 0 & \sin \varphi_B & 0 \\ 0 & 1 & 0 & 0 \\ -\sin \varphi_B & 0 & \cos \varphi_B & 0 \\ 0 & 0 & 0 & 1 \end{bmatrix}, \\ \mathbf{M}_{56} = \begin{bmatrix} 1 & 0 & 0 & 0 \\ 0 & \cos \Sigma_{wh} & -\sin \Sigma_{wh} & 0 \\ 0 & \sin \Sigma_{wh} & \cos \Sigma_{wh} & 0 \\ 0 & 0 & 0 & 1 \end{bmatrix}, & \mathbf{M}_{45} = \begin{bmatrix} 1 & 0 & 0 & 0 \\ 0 & 1 & 0 & 0 \\ 0 & 0 & 1 & L_z \\ 0 & 0 & 0 & 1 \end{bmatrix}, & \mathbf{M}_{34} = \begin{bmatrix} 1 & 0 & 0 & -E_{wh} \\ 0 & 1 & 0 & 0 \\ 0 & 0 & 1 & 0 \\ 0 & 0 & 0 & 1 \end{bmatrix}, \\ \mathbf{M}_{w3} = \begin{bmatrix} \cos \varphi_w & \sin \varphi_w & 0 & 0 \\ -\sin \varphi_w & \cos \varphi_w & 0 & 0 \\ 0 & 0 & 1 & 0 \\ 0 & 0 & 0 & 1 \end{bmatrix}; & \mathbf{M}_{wh} \text{ denotes the transfor-} \end{matrix}$$

tion matrix of S_h to S_w ; \mathbf{L}_{wh} denotes the 3×3 upper-left submatrix of \mathbf{M}_{wh} ; Σ_{wh} denotes the axis intersection angle between the honing wheel and gear; E_{wh} denotes the center distance between the honing wheel and work gear; φ_B denotes the rotation angle of the tool holder swing axis of the honing wheel; φ_w denotes the rotation angles of the work gear. L_z denotes the axial feed of the honing wheel provided by

$$\varphi_w(\varphi_h, L_z) = \frac{N_h}{N_w} \varphi_h + \frac{\tan \beta_w}{r_{w1}} L_z, \tag{13}$$

$$\Sigma_{wh} = \beta_h \pm \beta_w, \tag{14}$$

$$E_{wh} = r_{h1} - r_{w1}, \tag{15}$$

where N_w denotes the number of teeth of the work gear, r_{w1} denotes the operating pitch radius of the work gear; and β_w denotes the helix angle of the work gear. Similar to the processes involved in dressing a honing wheel with a diamond-dressing wheel, axial motion is added during the meshing of the honing wheel with the work gear. Generating the honing motion involves two kinematic parameters: L_z and φ_h . According to the gear meshing principle, the equation for meshing between the surfaces of the honing wheel and work gear can be derived [21, 23]

$$f_2(L_z, \varphi_h, \varphi_d, \theta, \lambda) = \mathbf{n}_w \cdot \frac{\partial \mathbf{r}_w}{\partial \varphi_h} = 0, \tag{16}$$

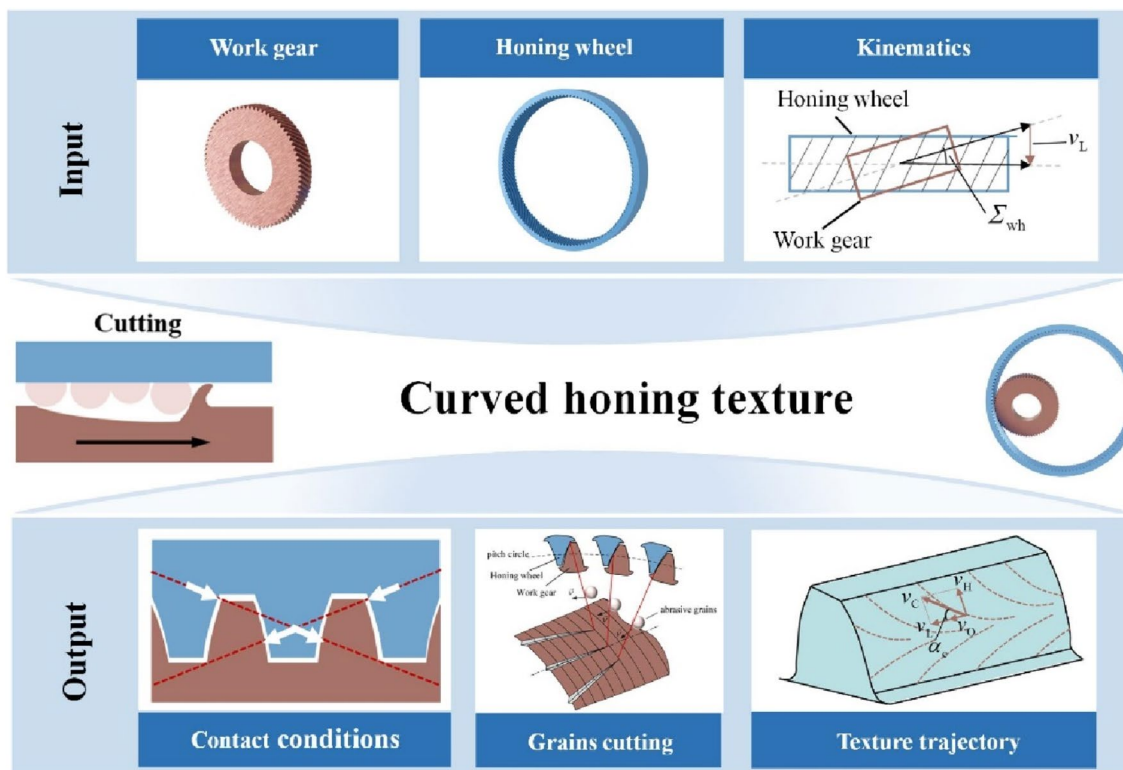


Fig. 4 Honing texture formation mechanism diagram

$$f_3(L_z, \varphi_h, \varphi_d, \theta, \lambda) = n_w \cdot \frac{\partial r_w}{\partial L_z} = 0. \tag{17}$$

By introducing the involute parameters θ and λ into the above meshing equation, φ_h and L_z of the contact points can be determined, and the position vector and normal vector of each discrete point of the work gear tooth surface can be determined using Eqs. (10) and (11).

3 Honing texture control based on variable axis intersection angle

3.1 Curved honing texture formation mechanism

During the honing process, the curved honing texture produced on the surface of the work gear primarily originates from the cutting motion between the abrasive grains distributed on the teeth of the honing wheel and work gear tooth surface. Therefore, the cutting speed direction is the dominant influence on the honing texture. In the process of honing the work gear, the motion of the honing wheel and work gear can be regarded as the meshing motion of a pair of staggered-axis helical gears. The honing wheel rotates and reciprocates along the axial direction, facilitating material removal from the entire tooth surface of the work gear. Based

on the motion relationship described, the cutting speed v_C is perceived to consist of the profile sliding speed rate v_H , lengthwise sliding speed rate v_L , and axial feed speed rate v_O , as depicted in Fig. 4. Given that the axial speed rate is considerably lower than the profile and lengthwise sliding speed rates, the axial feed speed can be disregarded [6].

Therefore, the cutting speed is derived from the vector combination of the profile sliding rate and lengthwise sliding rate, as given by Eq. (18). The profile sliding rate v_H is determined by the radius of curvature for both the honing wheel (ρ_H) and work gear (ρ_W) at their contact point, and by the angular velocities of the honing wheel (ω_H) and work gear (ω_W), as illustrated in Eq. (19). The lengthwise sliding speed is influenced by the work gear's circumferential speed ω_W , honing wheel's helix angle β_H , distance from the contact point r_W , and intersection angle Σ_{wh} between the axes of the work gear and honing wheel, as shown in Eq. (20). The cutting speed direction, α_c , is determined by the angle between the profile sliding feed rate and lengthwise sliding rate, as Eq. (21) [25].

$$v_C = \sqrt{v_L^2 + v_H^2}, \tag{18}$$

$$v_H = \rho_W \omega_W - \rho_H \omega_H. \tag{19}$$

$$v_L = r_w \omega_w \frac{\sin \Sigma_{wh}}{\cos \beta_H}, \tag{20}$$

$$\alpha_c = \arctan \left(\frac{v_H}{v_L} \right). \tag{21}$$

According to Eq. (19), the profile sliding rate v_H is zero at the position of the work gear pitch circle, and the profile sliding rate increases gradually on both sides of the pitch circle in the opposite direction. Based on Eq. (20), the lengthwise sliding rate is related to the distance r_w from the contact point of the work gear to the axis and the helix angle β_H of the honing wheel. Therefore, the size and direction of the cutting speed at any point on the tooth surface of the workpiece are not the same, which disturbs the honing texture in an arc; this structure is also called the “herringbone” structure [8]. As the work gear and honing wheel are in line contact during honing, a line model of the work gear contact during honing is required to establish the honing texture of the work gear surface. Additionally, the axial feeding motion L_z of the honing wheel aims to avoid uneven material removal from the workpiece surface, which has a relatively weak effect on the lengthwise sliding velocity of the contact point and can be ignored [6]. In the conventional honing process, φ_B defaults to 0. The teeth of the work gear are formed by the envelope of the honing wheel teeth; therefore, the parameters of the work gear are the same as those of the diamond dressing wheel used for dressing the honing wheel. Using the fixed coordinate system $S_w(x_w, y_w, z_w)$ as a reference analysis, the cutting speed of the abrasive grain at any contact point with the tooth surface of the work gear v_{wh} (with the same meaning as v_C , the difference is that v_{wh} facilitates a quantitative calculation) is expressed as

$$v_{wh} = \mathbf{w}_w \mathbf{r}_w - \mathbf{w}_h \mathbf{r}_h = \begin{bmatrix} -y\omega_w + \omega_h(y \cos \Sigma_{wh} + z \sin \Sigma_{wh}) \\ x\omega_w - \omega_h(x + E_{wh}) \cos \Sigma_{wh} \\ -\omega_h(x + E_{wh}) \sin \Sigma_{wh} \end{bmatrix}, \tag{22}$$

where \mathbf{w}_w and \mathbf{w}_h denote the angular velocity of the contact point of the work gear and honing wheel, respectively, and $x, y,$ and z are the components of the position vector of the contact point M' in the fixed coordinate system S_w of the work gear.

The calculated results for the cutting speed and normal vector at any contact point between the work gear tooth surface and honing wheel tooth surface were integrated. The following equation represents the condition where the honing-wheel tooth surface and workpiece tooth surface sustain conjugate meshing

$$\begin{aligned} & (E_{wh} p \cos \Sigma_{wh} - r_b^2 \sin \Sigma_{wh}) \cos (\sigma_0 + \theta + \lambda + \varphi_w) \\ & + (\theta p^2 - \lambda r_b^2) \sin \Sigma \sin (\sigma_0 + \theta + \lambda + \varphi_w) \\ & + (p \cos \Sigma_{wh} - E_{wh} \sin \Sigma_{wh} - p N_h / N_w) r_b = 0. \end{aligned} \tag{23}$$

The contact line equation is obtained by combining Eqs. (10) and (23). The position and normal vectors of any point on the contact line of the work gear can be determined using φ_w .

3.2 Prediction and 3D modeling of curved honing texture

Using the aforementioned mathematical model, the honing texture was simulated, enabling predictions on how the abrasive grains of the honing wheel and honing motion influence the texture. For computational simplicity in modeling the honing texture, certain influencing factors were omitted. These include machining chatter, deviations in assembly and motion of the machining shaft, and thermal deformations of the honing wheel and work gear. It was also assumed that all abrasive grains were rigid, spherical, of uniform diameter, and securely affixed to the honing wheel, with no consideration given to grain fracture or wear during the honing process.

As shown in Fig. 5, the calculation steps of the honing texture are divided into five stages: in the first stage, the work gear tooth surface is observed along the profile direction (u), starting from the engagement’s onset and spanning an angle of equal parts during the engagement process. This yields several contact lines on the tooth surface in the lengthwise direction (v) with equidistant points. Each grid point represents the contact point between an abrasive grain and the work gear. At each contact point, the calculation determines the direction of the abrasive grain’s velocity. In the second stage, given that the abrasive grains move in the direction of cutting velocity, a two-dimensional texture trajectory is simulated. This is achieved by further refining the partitioning of the tooth surface mesh and aligning the cutting velocity direction at each contact point. In the third stage, it is assumed that the abrasive grains’ center points are situated on the grid points, allowing them to move a short distance in the cutting speed direction. The fourth stage involves calculating the textural cross-sectional attributes of abrasive particles on the tooth surface. For any grid point within the spherical particle’s domain, the associated interference depth h_i can be determined

$$h_i = \sqrt{\left(\frac{d_{gr}}{2}\right)^2 - r_i^2}, \tag{24}$$

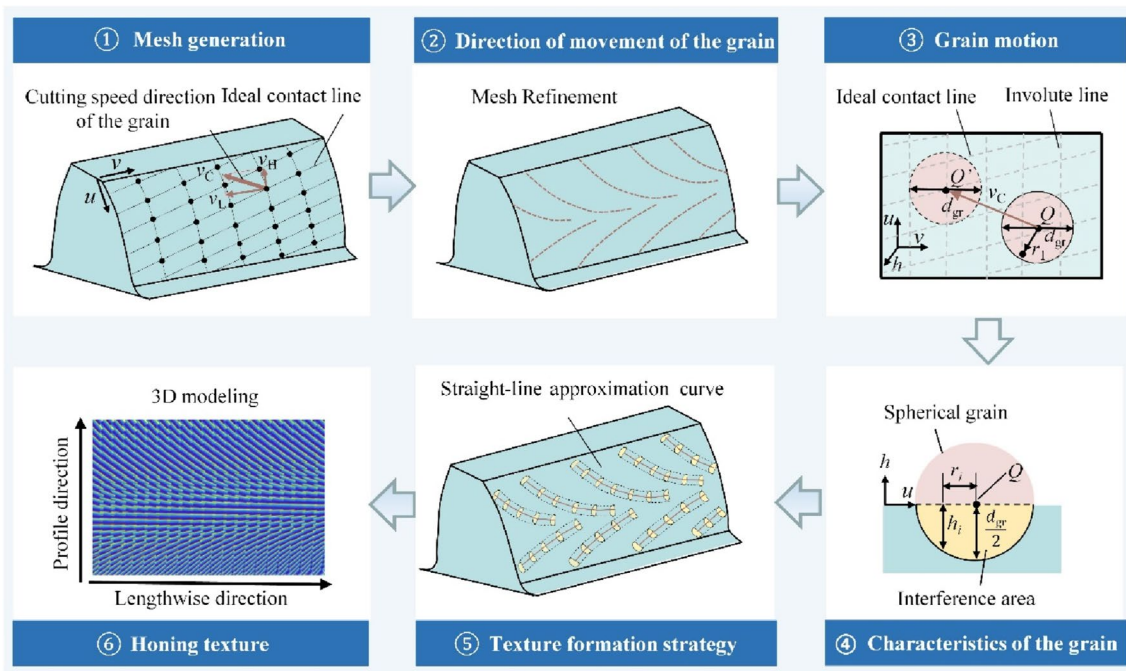


Fig. 5 Calculation process of honing texture

where r_i denotes the distance between point i , and points Q and d_{gr} correspond to the diameter of the spherical abrasive grain.

In the fifth stage, the trajectory of the abrasive grains, as they move a short distance in the direction of the cutting speed at each grid point's contact position, is determined. A method employing discrete motion trajectories for the abrasive grains is utilized. This method involves approximating the entire curve using numerous discrete linear trajectory segments, thereby allowing for an approximate simulation of the 3D curved honing texture.

3.3 Control method of honing texture change trend

The curved texture created through honing effectively reduces noise, and directly controlling this texture on the gear surface is crucial for achieving the optimal texture. As evident from Sect. 3.1, the formation of this texture arises from the cutting motion of the abrasive grain, moving in the direction of the cutting speed at the contact point, which in turn creates scratches on the tooth surface. Given that honing wheel tools require continuous dressing with diamond dressing wheels during their service life, the diameter of the honing wheel will vary, which requires controlling the geometry of the honing wheel by adjusting the intersection angle Σ_{hd} between the diamond dressing wheel and honing wheel's axis. Additionally, the variations in the axis intersection angle Σ_{hd} lead to a variation in the helix angle of the honing wheel, which makes the axis

intersection angles Σ_{wh} and Σ_{hd} as equal. According to Eq. (22), the axis intersection angle Σ_{wh} and center distance E_{wh} contribute to the cutting speed's size and direction at the tooth surface's contact point. Therefore, by actively adjusting the axis intersection angle Σ_{hd} , the direction of the texture can be controlled. The axis intersection angle Σ_{hd} serves as a function of the center distance E_{hd} . The function relationship is

$$\Sigma_{hd} = \arccos \frac{(\omega_d/\omega_h)r_{d1} \cos \beta_d}{r_{d1} + E_{hd} + \Delta E_{hd}} - \beta_d, \tag{25}$$

where ω_d denotes the angular speed of the diamond-dressing wheel; ω_h denotes the angular speed of the honing wheel; and ΔE_{hd} denotes the radial dressing amount of the honing wheel. Given that the spreading motion relationship of each motion axis does not change during honing, a change in the axis intersection angle does not affect the tooth surface accuracy. Taking an involute line at the end face of the gear as the research object, we analyzed the changing law of the size and direction of the cutting speed of the contact point from the root to the top of the tooth by changing the axis intersection angle during honing-wheel processing. The results show that the cutting speed direction on the gear tooth surface is unevenly distributed on both sides of the pitch circle, and with an increase in the axis intersection angle, the gear pitch circle position remains basically unchanged. Furthermore, the angle between the cutting speed of the abrasive grain at each contact point and tooth direction continues to increase,

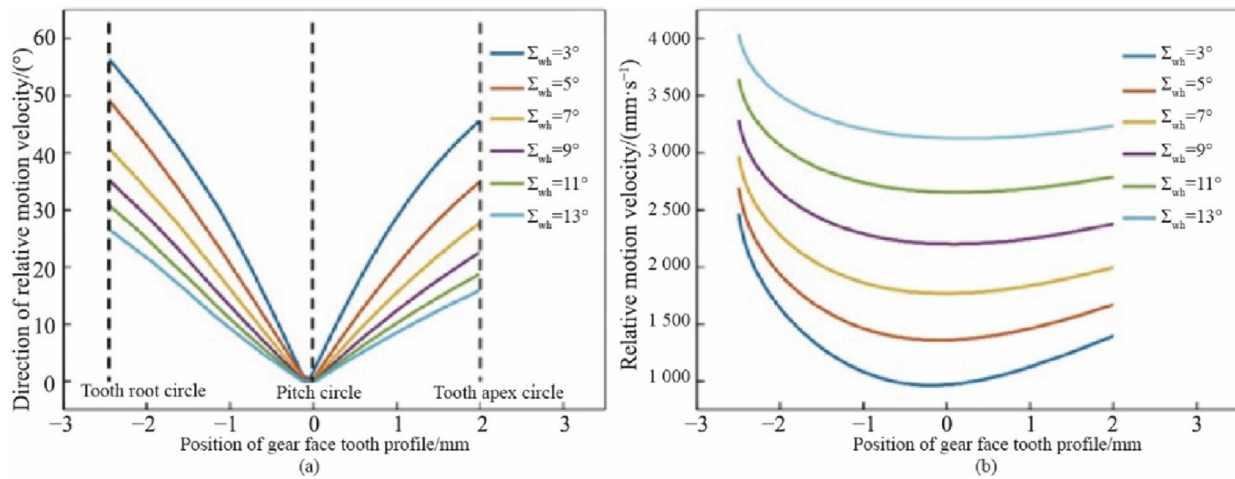


Fig. 6 Influence law of axial intersection angle on cutting speed **a** influence of the direction of cutting speed, **b** influence of cutting speed magnitude

as shown in Eqs. (19)–(21). This occurs because, as the contact point moves further from the pitch circle position, the growth rate of the profile sliding rate exceeds that of the lengthwise sliding rate, as depicted in Fig. 6a.

The abrasive grains’ cutting speed at every contact point across the entire involute varied as the position of the contact point shifted. The cutting speed from the root to the tooth’s top first decreased, then increased. Moreover, the speed difference from the tooth’s bottom to its top consistently decreased, enhancing the stability of the honing process. This consistency avoids periodic shifts in honing force throughout the process, extending the honing wheel’s lifespan. Furthermore, with a rise in the axis intersection angle, there was a continuous increase in the cutting speed between the abrasive grain and the work gear tooth surface. At an axis intersection angle of 13°, the maximum cutting speed of the abrasive grains remains below 5 000 mm/s, which is less than the speed produced during grinding, as illustrated in Fig. 6b [25, 26]. Consequently, within the chosen range of axis intersection angle for this research, augmenting the angle can both alter the abrasive grain’s cutting speed direction at the contact point and enhance the material removal rate, while effectively preventing any burning on the tooth surface.

4 Flexible topology modification of internal gearing power honing based on multi-axis linkage

4.1 Additional motion axis setting and tooth surface normal deviation

To achieve gear surface topology modification, the multi-axis linkage relationship during the operation of the honing

machine can be expressed as a polynomial and by optimizing the polynomial coefficients, thus achieving arbitrary topology modification of the work gear surface without the need for a new custom-made diamond dressing wheel. Therefore, in this study, the feed E_{wh} of the radial feed shaft (X -axis) of the honing wheel, rotation angle Σ_{wh} of the cross shaft (A -axis) between the honing wheel and the work gear, and rotation angle φ_B of the tool holder of the honing wheel are defined as the fifth-order polynomials with respect to the axial feed axial (Z_1 -axis)) motion L_z of the honing wheel

$$\begin{cases} E_{wh}(L_z) = E_{wh} + \sum_{k=0}^5 a_k L_z^k, \\ \Sigma_{wh}(L_z) = \Sigma_{wh} + \sum_{k=0}^5 b_k L_z^k, \\ \varphi_B(L_z) = \sum_{k=0}^5 c_k L_z^k. \end{cases} \quad (26)$$

Among them, the polynomial coefficients a_0 – a_5 , b_0 – b_5 , and c_0 – c_5 are the dynamic parameters used to modify the topology during the honing modification process, with a total of 18 parameters, which are denoted as λ_j ($j = 1$ –18) in the sequence in the later section. When processing standard involute helical work gears with the honing wheel (where the work gears are not subject to modification), it is appropriate to set the polynomial coefficients of these axes to zero. Utilizing the flexible modification method introduced in this study, the mathematical model for tooth surface modification elucidates the relationship between the polynomial coefficients of the honing machine’s supplementary motion and adjusted tooth surface. To refine the tooth surface irregularities, one can adjust the polynomial coefficients of the X -axis, A -axis, and B -axis

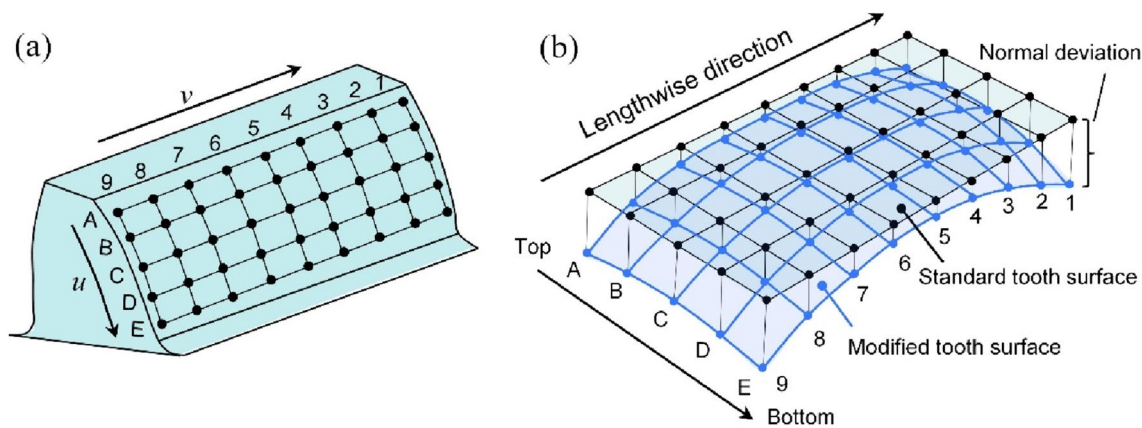


Fig. 7 Schematic diagram of the definition **a** mesh of gear tooth surface, **b** morphology of gear tooth surface

progressively. This allows the altered tooth surface to closely align with the intended target, thereby enhancing the precision of the modified surface.

The additional movement of each axis directly results in the contour discrepancy between the theoretical standard tooth surface and actual modified tooth surface. To depict the variation between these surfaces, it is pertinent to introduce the concept of normal tooth surface deviation. As illustrated in Fig. 7a, the topology modification of the tooth surface, consisting of 45 grid points ($i = 45$), is defined on one side of the tooth surface. This aids in calculating the normal deviation from points on the theoretical standard tooth surface for the one-sided work gear modification. Figure 7b portrays the theoretical standard tooth surface as a flat grid delineated by slender black lines, serving as a benchmark to contrast against the modified tooth surface. Conversely, the modified tooth surface is depicted as a contoured grid with prominent blue lines. The normal deviation at each grid point between the modified and standard tooth surfaces is computed as [27]

$$\delta\epsilon = (\mathbf{r}_w - \mathbf{r}_s) \cdot \mathbf{n}_s, \tag{27}$$

where \mathbf{r}_s and \mathbf{n}_s denote the position vector and normal vector of the standard tooth surface, respectively.

4.2 Solution of polynomial coefficients based on least squares algorithm

To realize the desired topology of the target modified tooth surface, a numerical least-squares estimation algorithm based on the sensitivity matrix was utilized. Through several closed-loop iterations, the polynomial coefficients of these supplementary movements were determined. The sensitivity matrix \mathbf{M}_s represents the partial derivative $\delta\epsilon_i$ of the tooth surface's normal deviation in relation to the change in the polynomial coefficient $\delta\lambda_j$. The deviation

shift $\delta\epsilon_i$ at point i equates to a linear combination of the change in the normal deviation $\delta\lambda_j$ caused by the variation in the polynomial coefficient, indicating the influence of each polynomial coefficient on the normal deviation of the modified tooth surface and standard theoretical tooth surface at all grid points [15]. Once the normal deviation of the target's modified tooth surface and sensitivity matrix are established, the pertinent polynomial coefficients can be obtained using the least-squares approach, as depicted in Eqs. (28) and (29).

$$\begin{aligned} \{\delta\epsilon_i\} &= \mathbf{M}_s \{\delta\lambda_j\} = \begin{bmatrix} \partial\epsilon_i \\ \partial\lambda_j \end{bmatrix} \cdot \{\delta\lambda_j\}, \\ i &= 1, 2, \dots, 45, j = 1, 2, \dots, 18, \end{aligned} \tag{28}$$

$$\{\delta\lambda_j\} = (\mathbf{M}_s^T \cdot \mathbf{M}_s)^{-1} \mathbf{M}_s \cdot \{\delta\epsilon_i\}, i = 1, 2, \dots, 45, j = 1, 2, \dots, 18. \tag{29}$$

Given that the sensitivity matrix is non-square and usually pathological, the singular value decomposition is applied to the pseudo-inverse of the sensitivity matrix \mathbf{M}_s to avoid computational divergence, and Eq. (29) can be further rewritten as [16]

$$\{\delta\lambda_j\} = \mathbf{V}\mathbf{W}^+ \mathbf{U}^T \cdot \{\delta\epsilon_i\}, i = 1, 2, \dots, 90, j = 1, 2, \dots, 18. \tag{30}$$

\mathbf{U} and \mathbf{V} contain a unitary matrix, and \mathbf{W} denotes a diagonal characteristic matrix whose diagonal elements are all non-negative real numbers. Matrix \mathbf{W}^+ denotes the pseudo-inverse of matrix \mathbf{W} , and \mathbf{U}^T denotes the transpose of matrix \mathbf{U} .

The specific calculation process of the polynomial coefficients is shown in Fig. 8. (a) Initialize the polynomial coefficients and set the higher-order polynomial coefficients to 0. (b) Input the normal deviation of the target modified tooth surface and current actual tooth surface. (c) Using Eq. (30) and the least-squares estimation

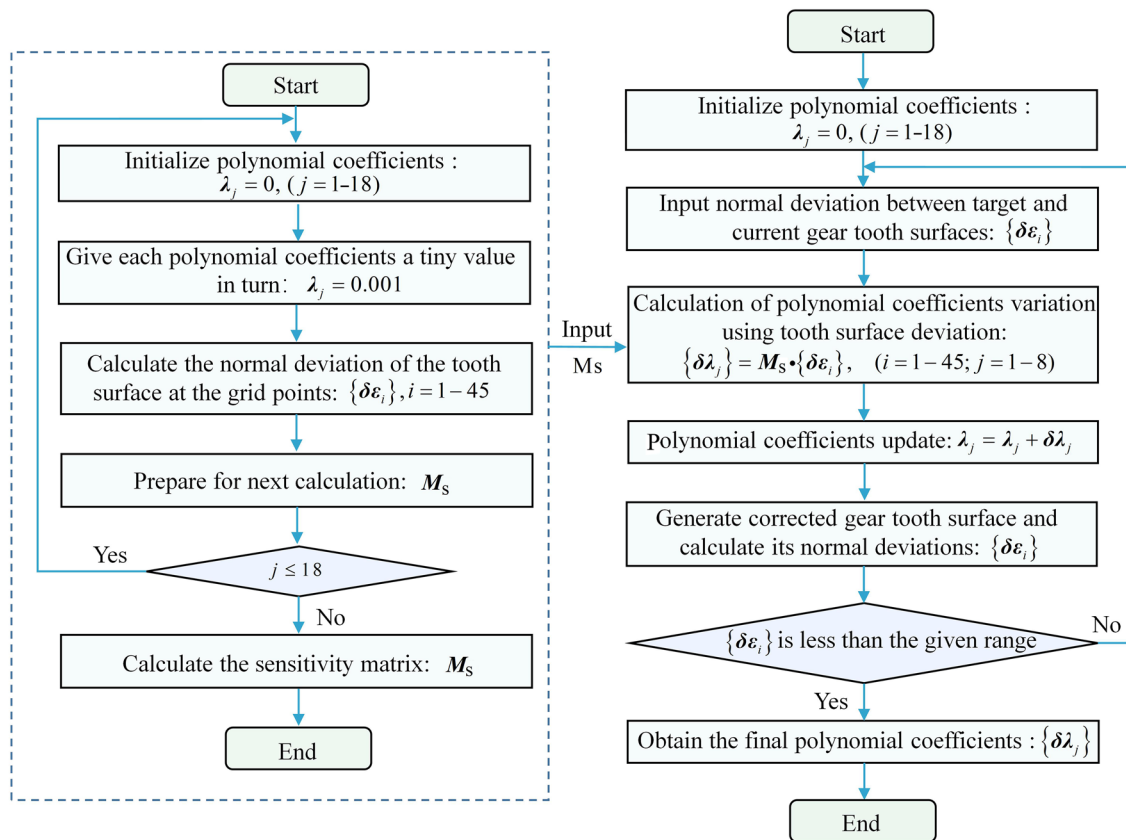


Fig. 8 Flow chart of optimization iteration calculation

method, calculate the variation in the polynomial coefficients. The sensitivity matrix is formed by introducing small changes (either 0.001 mm or 0.001°) to each polynomial coefficient individually, keeping all others constant. This results in a linear combination, showcasing how the normal deviation responds to adjustments in specific coefficients, using the coefficients' partial differentiation sequence. (d) Superimpose the polynomial coefficients obtained in the previous step to generate new polynomial coefficients. (e) Calculate the modified tooth surface under the influence of polynomial coefficients using Eqs. (10–12), (15–16), and (26), and calculate the tooth surface deviation between the current modified tooth surface and target modified tooth surface by Eq. (27). (f) Determine whether the normal deviation of tooth surface under the influence of the polynomial coefficients satisfies the tolerance value. If it does, then cease iterations and present the polynomial coefficients for each axis. If it does not, then proceed to the next step. (g) Calculate the amount of change in the polynomial coefficients based on the currently updated normal deviation, and calculate the normal deviation again until it is less than the given range or remains constant.

5 Numerical examples and discussion

5.1 Tooth surface topology modification based on additional motion

The primary parameters for the diamond-dressing wheel, honing wheel, and work gear used in the numerical simulation are listed in Table 1. To validate the efficiency of the closed-loop topology modification technique for helical gears, Table 2 presents the normal deviation data (the topology modification amount) between the provided target modified tooth surface and theoretical standard tooth surface. The topographical distribution of the normal deviations for both left and right sides of the target modified tooth surface is visualized using this data. This distribution is depicted in Fig. 9a. The deviations in both the tooth profile and upward tooth direction exhibit a parabolic contour, characterized by a pronounced center and diminishing sides. The peak normal deviation registers at 24.2 μm at the tooth surface extremities, whereas the nadir corresponds to 5.57 μm around the tooth surface's midpoint.

The sensitivity matrix, sized at 45×18, can be described as follows. Owing to the necessity of recalculating the

Table 1 Parameters for the diamond dressing tool, honing wheel, and work gear

Parameters	Dressing tool	Honing wheel	Work gear
Number of teeth (N_g)	39	123	39
Normal module (m_n)	2	2	2
Normal pressure angle (α_n)	20	20	20
Face width	20	30	20
Helix angle	20° (left)	25°/27°/29°/31° (left)	20° (left)
Tip diameter	87.005 8	288.056 4	87.005 8
Root diameter	78.005 8	297.056 4	78.005 8

Table 2 Data for normal deviations of target tooth surface topography

Tip	Unit: μm								
A	-24.19	-17.72	-10.38	-8.68	-5.57	-8.68	-10.38	-17.72	-24.19
B	-19.10	-13.09	-8.67	-5.82	-4.56	-5.82	-8.67	-13.09	-19.10
C	-16.10	-10.36	-6.17	-3.51	-2.48	-3.51	-6.17	-10.36	-16.10
D	-19.10	-13.09	-8.67	-5.82	-4.56	-5.82	-8.67	-13.09	-19.10
E	-24.19	-17.72	-10.38	-8.68	-5.57	-8.68	-10.38	-17.72	-24.19
Root	9	8	7	6	5	4	3	2	1

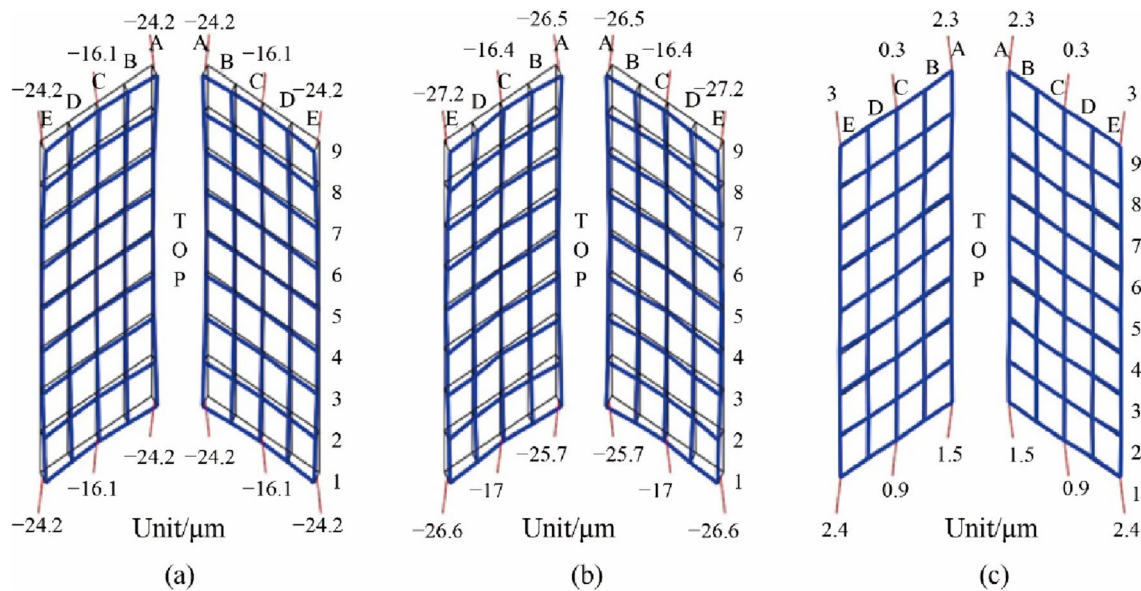


Fig. 9 Results of tooth surface modification **a** target tooth surface, **b** actual tooth surface, and **c** modification error

normal deviation of the modified tooth surface from its target during every iteration, the least squares method based on the sensitivity matrix might cause multiple calculations to diverge from the expected results. Post several closed-loop iterations and with additional motions applied to the X -, A -, and B -axes, the analysis reveals an optimal

topologically-modified tooth surface, depicted in Fig. 9b. A selection of the optimal polynomial coefficients can be detailed in Table 3. The subsequent modification error outcomes are illustrated in Fig. 9c. Impressively, the maximum modification error remains below 5 μm , fulfilling the stipulated modification accuracy standards.

Table 3 Polynomial coefficients for additional motion

Coefficients	Value	Coefficients	Value	Coefficients	Value
λ_1	-3.15×10^{-4}	λ_7	2.51×10^{-4}	λ_{13}	2.61×10^{-5}
λ_2	9.69×10^{-4}	λ_8	-7.42×10^{-4}	λ_{14}	-4.36×10^{-5}
λ_3	-7.39×10^{-3}	λ_9	-3.67×10^{-3}	λ_{15}	-5.16×10^{-5}
λ_4	7.74×10^{-3}	λ_{10}	-1.88×10^{-3}	λ_{16}	6.97×10^{-5}
λ_5	9.31×10^{-3}	λ_{11}	3.01×10^{-3}	λ_{17}	9.63×10^{-5}
λ_6	9.64×10^{-3}	λ_{12}	5.15×10^{-3}	λ_{18}	-1.42×10^{-4}

$$M_s = \begin{bmatrix} 7.0650 & 2.8630 & \dots & 23.0592 & -16.6729 \\ 0.9461 & 0.3055 & \dots & 3.7984 & -2.1518 \\ \vdots & \vdots & \ddots & \vdots & \vdots \\ 10.9774 & 3.6065 & \dots & 33.9397 & -22.0411 \\ 7.7394 & 2.9124 & \dots & 25.6276 & -16.4206 \end{bmatrix}_{45 \times 18} \quad (31)$$

5.2 Prediction and active regulation of modified honing textures

Existing literature on curved honing textures is limited. However, it remains imperative to both predict and actively manage the honing texture post-modification. Although topology modification is achieved by introducing only a minor motion to the machine axis, the meshing principle is still applicable. Incorporating the modified tooth surface equations, influenced by the polynomial coefficients, into Eqs. (22) and (23), the

honing texture modeling approach aligns with the one presented in Sect. 3. When the intersection angle of the axes is set at 5° , the surface morphology of the tooth surface is depicted in Fig. 10. Notably, the tooth surface’s curved honing texture adopts a “herringbone” pattern on both sides of the pitch circle. Comparative analysis indicates that the modified honing texture, influenced by the additional motion, remains largely consistent with the texture prior to modification. This suggests that introducing a minor supplementary movement does not materially alter the honing texture.

Given that a minor adjustment in each axis does not alter the honing texture, it is evident from Sect. 3 that the honing texture direction of work gear tooth surface is determined by the cutting speed direction. By tweaking the helix angle of the honing wheel during the diamond dressing phase, the axis intersection angle between the honing wheel and workpiece was adjusted. Consequently, the cutting speed direction was altered, thereby changing the honing texture

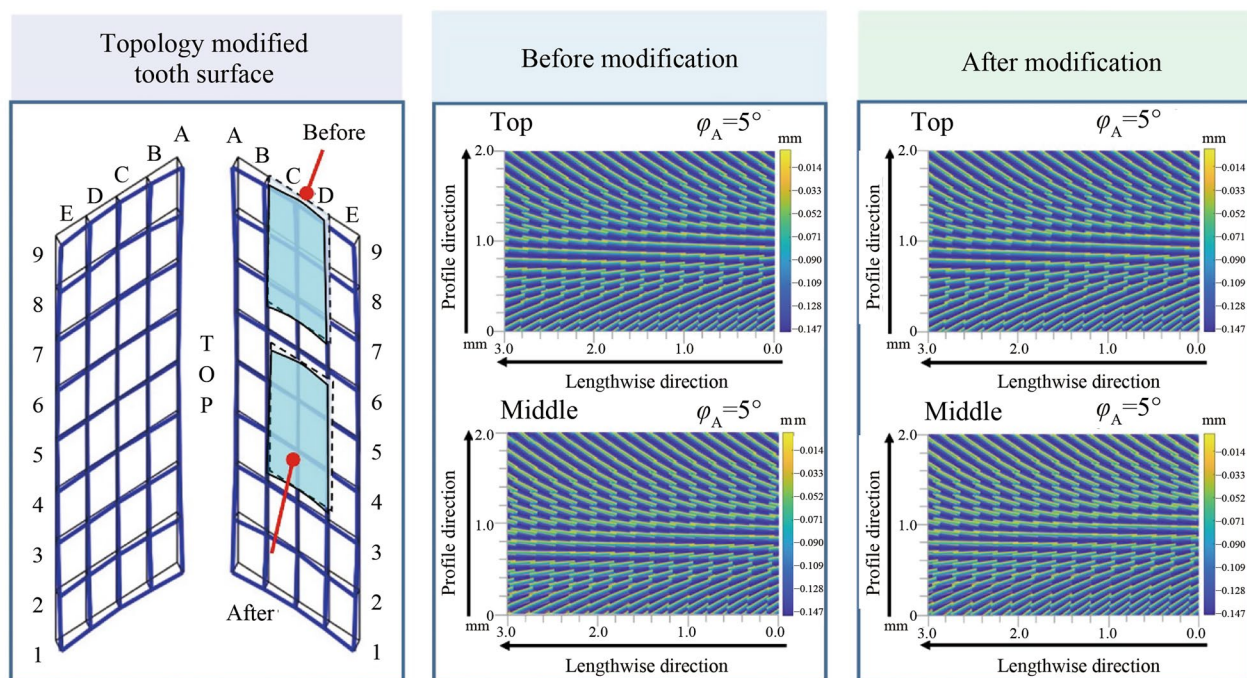


Fig. 10 Comparison of honing texture before and after modification

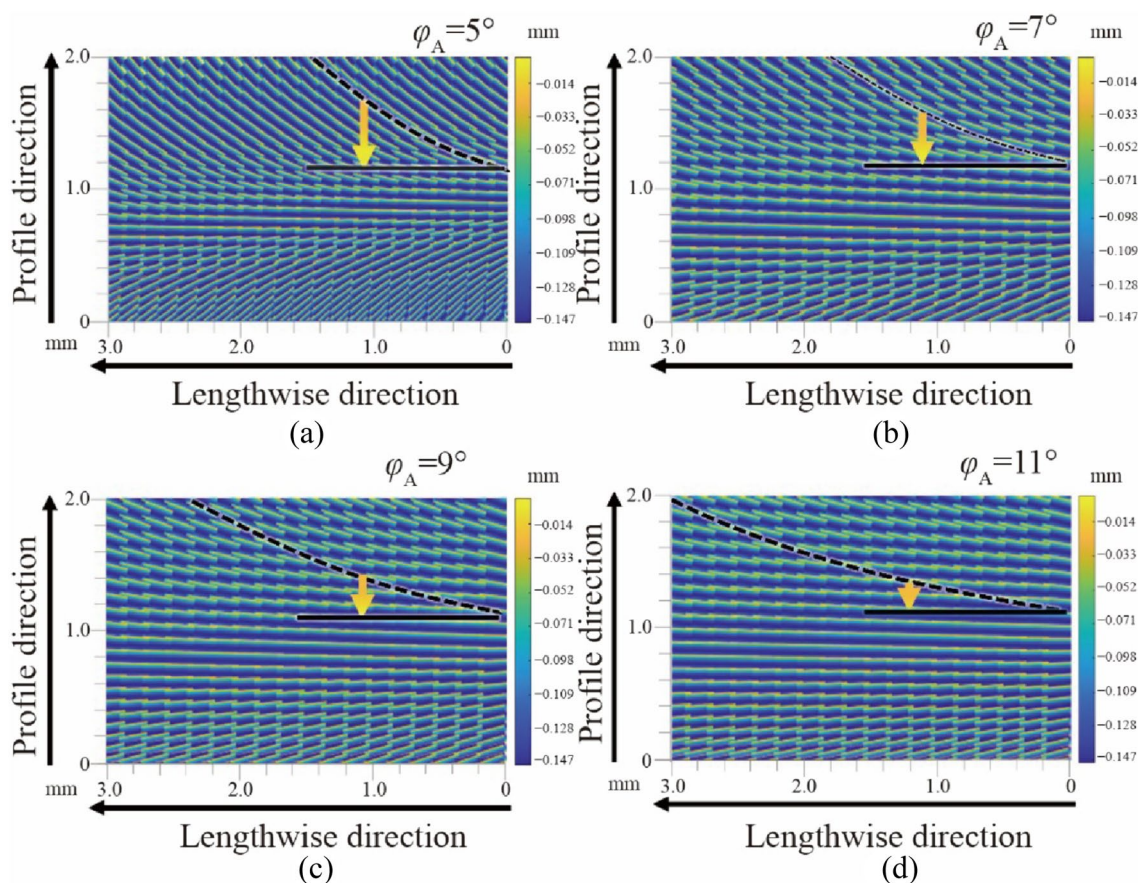


Fig. 11 Effect of different axis intersection angles on modified honing texture

of the work gear without affecting its tooth geometry. Unlike grinding, honing entails a linear contact; any direct alteration in the axial intersection angle between the honing wheel and work gear, particularly during topology modification, can lead to significant damage to the honing wheel [28]. Hence, during the dressing of honing wheels using diamond-dressing wheels, the honing texture is modified by adjusting the helix angle of the honing wheel.

As illustrated in Fig. 11, when we assume that all honing wheels are comprised of spherical grains with a consistent diameter of 0.3 mm, altering the axis intersection angle between the honing wheel and work gear (at angles of 5° , 7° , 9° , and 11°) yields specific outcomes. The results indicate that a smaller axis intersection angle between the honing wheel and work gear results in a more pronounced shift in the modified honing texture of the work gear. In this case, the texture direction increasingly leans toward the profile direction. Conversely, as the axial intersection angle increases, the tendency of the modified honing texture to change reduces, with the texture direction steadily aligning with the lengthwise direction. Thus, this research offers a practical approach to predict and manage surface texture during honing through topology modification.

6 Conclusions

In modern gearing applications, both topology modification and tooth surface texture play pivotal roles in reducing gear noise. This study introduces a novel manufacturing technique for high-order modified helical gears, delving into the laws governing the formation and modeling of honing textures. Furthermore, the research presents an innovative method for 3D modeling and controlling the modified honing texture.

Employing flexible topology modification, various parameters—namely the feed of the honing wheel's radial feed axis, the rotation angle of the honing wheel and work gear's intersection axis, and the oscillation axis rotation angle of the honing-wheel tool holder—are conceptualized as high-order polynomials in relation to the honing wheel's axial feed axis. Adjusting the coefficients of these high-order polynomials facilitates precision gear modifications, predicts the modified honing texture, and enables active texture control by adjusting the honing wheel's helix angle during its diamond-dressing phase. Crucially, the additional motion imparted for topology modification does not alter the direction of the honing texture. Instead, the texture's direction consistently correlates with the axis intersection angle between the honing wheel and work

gear, both pre- and post-modification. A larger intersection angle positions the modified honing texture closer to the lengthwise direction, while a smaller one shifts it toward the profile direction. This methodology establishes a foundational framework for investigating how different honing textures influence vibration and noise reduction. It offers valuable theoretical insights and directions for exploring the coordinated control of gear shape and tooth texture, furthering advancements in gear vibration and noise mitigation.

Acknowledgements This study was supported by the National Natural Science Foundation of China (Grant Nos. 52075142, U22B2084, and 52275483).

References

- Gao P, Liu H, Yan P et al (2022) Research on application of dynamic optimization modification for an involute spur gear in a fixed-shaft gear transmission system. *Mech Syst Signal Process* 181:109530. <https://doi.org/10.1016/j.ymssp.2022.109530>
- Yadav RD, Singh AK (2019) International journal of machine tools and manufacture a novel magnetorheological gear profile finishing with high shape accuracy. *Int J Mach Tools Manuf* 139:75–92
- Gupta N, Tandon N, Pandey RK (2018) An exploration of the performance behaviors of lubricated textured and conventional spur gearsets. *Tribol Int* 128:376–385
- Tran VQ, Wu YR (2018) Dual lead-crowning for helical gears with long face width on a CNC internal gear honing machine. *Mech Mach Theory* 130:170–183
- Choi C, Ahn H, Yu J et al (2021) Optimization of gear macro-geometry for reducing gear whine noise in agricultural tractor transmission. *Comput Electron Agric* 188:106358. <https://doi.org/10.1016/j.compag.2021.106358>
- Guo Z, Li Y, Guo WC et al (2022) Research on the mechanisms of internal gear honing by use of cone-shape honing wheel with tool tilt angle. *Int J Adv Manuf Technol* 121:8187–8196
- Amini N, Westberg H, Klocke F et al (1999) An experimental study on the effect of power honing on gear surface topography. *Gear Technol* 16:11–18
- Brecher C, Schrank M, Kampka M et al (2019) Prediction of process forces in gear honing. *Gear Technol* 3:34–38
- Yuan B, Han J, Wang D et al (2017) Modeling and analysis of tooth surface roughness for internal gearing power honing gear. *J Braz Soc Mech Sci Eng* 39:3607–3620
- Chen C, Tang J, Chen H et al (2017) Research about modeling of grinding workpiece surface topography based on real topography of grinding wheel. *Int J Adv Manuf Technol* 93:2411–2421
- Miller M, Sutherland JW, Salisbury EJ et al (2001) A three-dimensional model for the surface texture in surface grinding, part 1: surface generation model. *J Manuf Sci Eng Trans ASME* 123:576–581
- Miller M, Sutherland JW, Salisbury EJ et al (2001) A three-dimensional model for the surface texture in surface grinding, part 2: grinding wheel surface texture model. *J Manuf Sci Eng Trans ASME* 123:582–590
- Zhou W, Tang J, Chen H et al (2018) Modeling of tooth surface topography in continuous generating grinding based on measured topography of grinding worm. *Mech Mach Theory* 131:189–203
- Yang YC, Wu YR, Tsai TM (2022) An analytical method to control and predict grinding textures on modified gear tooth flanks in CNC generating gear grinding. *Mech Mach Theory* 177:105023. <https://doi.org/10.1016/j.mechmachtheory.2022.105023>
- Wang C (2021) Multi-objective optimal design of modification for helical gear. *Mech Syst Signal Process* 157:107762. <https://doi.org/10.1016/j.ymssp.2021.107762>
- Shih YP (2010) A novel ease-off flank modification methodology for spiral bevel and hypoid gears. *Mech Mach Theory* 45:1108–1124
- Fonseca DJ, Shishoo S, Lim TC et al (2005) A genetic algorithm approach to minimize transmission error of automotive spur gear sets. *Appl Artif Intell* 19:153–179
- Tian X, Li D, Huang X et al (2022) A topological flank modification method based on contact trace evaluated genetic algorithm in continuous generating grinding. *Mech Mach Theory* 172:104820. <https://doi.org/10.1016/j.mechmachtheory.2022.104820>
- Shih YP, Chen SD (2012) A flank correction methodology for a five-axis CNC gear profile grinding machine. *Mech Mach Theory* 47:31–45
- Shih YP, Fong ZH (2017) Flank modification methodology for face-hobbing hypoid gears based on ease-off topography. *J Mech Des* 129:1294–1302
- Han J, Zhu Y, Xia L et al (2018) A novel gear flank modification methodology on internal gearing power honing gear machine. *Mech Mach Theory* 121:669–682
- Yu B, Shi Z, Lin J (2017) Topology modification method based on external tooth-skipped gear honing. *Int J Adv Manuf Technol* 92:4561–4570
- Tran VQ, Wu YR (2020) A novel method for closed-loop topology modification of helical gears using internal-meshing gear honing. *Mech Mach Theory* 145:103691. <https://doi.org/10.1016/J.mechmachtheory.2019.103691>
- Choe TC, Ri CN, Jo MJ et al (2022) Research on the engagement process and contact line of involute helical gears. *Mech Mach Theory* 171:104778. <https://doi.org/10.1016/j.mechmachtheory.2022.104778>
- Bergs T (2018) Cutting force model for gear honing. *CIRP Ann* 67:53–56
- Karpuschewski B, Knoche HJ, Hipke M (2008) Gear finishing by abrasive processes. *CIRP Ann Manuf Technol* 57:621–640
- Han J, Zhu Y, Xia L et al (2019) Influences of control error and setting error on machining accuracy of internal gearing power honing. *Int J Adv Manuf Technol* 100:225–236
- Brinksmeier E, Schneider C (1997) Grinding at very low speeds. *CIRP Ann* 46:223–226

Springer Nature or its licensor (e.g. a society or other partner) holds exclusive rights to this article under a publishing agreement with the author(s) or other rightsholder(s); author self-archiving of the accepted manuscript version of this article is solely governed by the terms of such publishing agreement and applicable law.



Jian-Ping Tang is currently studying in the School of Mechanical Engineering, Hefei University of Technology, Doctor degree candidate. His main research interests are in the exploration of gear textures.



Jiang Han received the B.S., M.S., and Ph.D. degrees in mechanical engineering from the Hefei University of Technology, Hefei, China. He is currently a Professor with the School of Mechanical and Engineering, Hefei University of Technology. His research interests include mechatronics, computer software and applications, numerical technology, and modern manufacturing systems and controls.



Guang-Hui Li is currently studying in the School of Mechanical Engineering, Hefei University of Technology, Doctor degree candidate. His main research direction is the study of gear honing process.



Xiao-Qing Tian received the B.Eng. and Ph.D. degrees in mechatronic engineering from the Hefei University of Technology, Hefei, China, in 2010 and 2014, respectively. She is currently a Professor with the School of Mechanical Engineering, Hefei University of Technology. Her research interests include gear machining precision control, gear modification, and soft material additive manufacturing.



Lian Xia received the B.S., M.S., and Ph.D. degrees in mechanical engineering from the Hefei University of Technology, Hefei, China. She is currently a Professor with the School of Mechanical and Engineering, Hefei University of Technology. Her research interests include mechatronics, computer-aided design, and modern manufacturing systems and controls.



Zhen-Fu Li is currently studying in the School of Mechanical Engineering, Hefei University of Technology Master's Degree candidate. His main research interests are in the exploration of gear textures.



Tong-Fei You is currently studying in the School of Mechanical Engineering, Hefei University of Technology, Doctor degree candidate. His main research direction is the exploration of machine tool machining errors.